New Journal of Physics
The open-access journal for physics

Advanced spectroscopic synchrotron techniques to unravel the intrinsic properties of dilute magnetic oxides: the case of Co:ZnO

A Ney[1,8], M Opel[2], T C Kaspar[3], V Ney[1], S Ye[1], K Ollefs[1], T Kammermeier[1], S Bauer[2], K-W Nielsen[2], S T B Goennenwein[2], M H Engelhard[3], S Zhou[4], K Potzger[4], J Simon[5], W Mader[5], S M Heald[6], J C Cezar[7], F Wilhelm[7], A Rogalev[7], R Gross[2] and S A Chambers[3]

[1] Fakultät für Physik and CeNIDE, Universität Duisburg-Essen, 47057 Duisburg, Germany
[2] Walther-Meißner-Institut, Bayerische Akademie der Wissenschaften, 85748 Garching, Germany
[3] Fundamental and Computational Sciences Directorate, Pacific Northwest National Laboratory, Richland, WA 99352, USA
[4] Institut für Ionenstrahlphysik und Materialforschung, Forschungszentrum Dresden-Rossendorf e.V., 01328 Dresden, Germany
[5] Institut für Anorganische Chemie, Rheinische Friedrich-Wilhelms-Universität, 53117 Bonn, Germany
[6] Advanced Photon Source, Argonne National Laboratory Argonne, IL 60439, USA
[7] European Synchrotron Radiation Facility (ESRF), 38043 Grenoble, France
E-mail: andreas.ney@uni-due.de

New Journal of Physics **12** (2010) 013020 (16pp)
Received 13 November 2009
Published 22 January 2010
Online at http://www.njp.org/
doi:10.1088/1367-2630/12/1/013020

Abstract. The use of synchrotron-based spectroscopy has revolutionized the way we look at matter. X-ray absorption spectroscopy (XAS) using linear and circular polarized light offers a powerful toolbox of element-specific structural, electronic and magnetic probes that is especially well suited for complex materials containing several elements. We use the specific example of $Zn_{1-x}Co_xO$ (Co:ZnO) to demonstrate the usefulness of combining these XAS techniques to unravel its intrinsic properties. We demonstrate that as

[8] Author to whom any correspondence should be addressed.

long as phase separation or excessive defect formation is absent, Co:ZnO is paramagnetic. We can establish quantitative thresholds based on four reliable quality indicators using XAS; samples that show ferromagnet-like behaviour fail to meet these quality indicators, and complementary experimental techniques indeed prove phase separation. Careful analysis of XAS spectra is shown to provide quantitative information on the presence and type of dilute secondary phases in a highly sensitive, non-destructive manner.

Contents

1. Introduction

The fabrication of dilute magnetic semiconductors (DMS) exhibiting intrinsic ferromagnetism at room temperature is currently a widely discussed issue in the material research community. It is of particular importance to avoid the formation of secondary magnetic phases because they significantly influence the magnetic properties of DMS [1]. Such phases are difficult to detect and lead to contradictory interpretations. In this context, $Zn_{1-x}Co_xO$ (Co:ZnO) has been heavily investigated as a candidate DMS after the prediction of ferromagnetism above 300 K [2]. Although many experimental reports claim room temperature ferromagnetic order [3]–[8], more recently an increasing number of publications describe its absence [9]–[12]. In particular, several groups have detected ferromagnetic behaviour only by integral superconducting quantum interference device (SQUID) magnetometry, although element-specific techniques fail to establish its presence [13, 14]. The possibility that magnetic nanoclusters play an important role in accounting for the observed magnetic behaviour is under discussion [15, 16] and cannot be ruled out, as shown recently by careful x-ray diffraction (XRD) analysis [12, 17] or depth-profiling x-ray photoelectron spectroscopy (XPS) [18]. Only in rare cases were such phase-separated clusters, which are well known from other transition metal-doped semiconductors like Mn:Ge [19, 20], directly imaged by cross-sectional transmission electron microscopy (TEM) [12]. Thus, a careful combined analysis of the structural and magnetic properties is required to exclude the possibility of phase separation and to establish an unambiguous interrelation between material properties and magnetism.

For the study of such complex magnetic materials, the power of x-ray absorption spectroscopy (XAS) is well known [21]. In addition, atom-specific sensitivity over a micron depth scale is available in the hard x-ray regime, allowing full characterization of epitaxial

films with a range of thicknesses as well as their interfaces to the substrate[9]. Near-edge XAS (XANES) reveals the oxidation state of the constituent atoms, and x-ray magnetic circular dichroism (XMCD) directly probes their magnetic properties [21]. The use of extended XAS fine structure (EXAFS), as well as x-ray linear dichroism (XLD) at the near edge, allows the local structural environment of even dilute species to be probed in a highly sensitive way. The power of XLD to quantitatively determine the fraction of absorbing atomic species incorporated at specific lattice sites was first demonstrated for Mn:GaN [23]. Combining the aforementioned techniques results in a unique experimental toolbox, particularly well suited for studying candidate DMS materials. While XANES [12, 15, 16, 18, 24], EXAFS [16, 18, 24, 25], soft XMCD [12]–[14], [26, 27] and hard XMCD [10, 27, 28] have often been employed in the study of Co:ZnO, XLD has very rarely been utilized, although this probe has provided valuable insights when used for Mn:GaN [23], Gd:GaN [29] and Co:ZnO [10, 13]. The high sensitivity, element specificity and non-destructive nature of these x-ray-based methods allow us to draw clear and unambiguous conclusions about the electronic, magnetic and structural properties on a local scale.

In this article, we report on the study of a comprehensive set of Co:ZnO epitaxial thin film samples fabricated using three deposition methods in four different laboratories. All samples have been analysed using an identical set of XAS and SQUID measurements. The key conclusion is that, contrary to numerous claims in the literature, phase-pure, crystallographically excellent Co:ZnO is uniformly paramagnetic (PM), irrespective of the preparation method. Ferromagnetic-like behaviour is observed only for samples showing extensive defect formation or phase separation, which is corroborated by complementary experimental techniques. We are able to identify the onset of phase separation using sophisticated x-ray-based techniques. Most importantly, we use quantitative information obtained by XLD to deconvolute XANES spectra and unravel the spectroscopic signatures of phase-separated material. These results correlate well with those from more traditional experimental techniques such as cross-sectional TEM. Based on our XAS measurements we define a quality threshold, given by four characteristic spectral features. Only if the sample quality exceeds these thresholds can the intrinsic properties of the specimen be probed. If not, the measured data may be strongly affected by extrinsic effects and phase separation becomes a concern. Taking this into account, we are able to establish a comprehensive understanding of the Co:ZnO system. This general approach can be applied to other candidate DMS materials, as well as dilute systems in general, in a straightforward manner.

2. Overview of the specimens and experimental details

A comprehensive set of $Co_xZn_{1-x}O(0001)$ epitaxial films in a thickness range from 100 to 350 nm was selected for our detailed spectroscopic study. The various samples were fabricated using four different growth methods; the sample names comprise information about the integral magnetic properties and the preparation method; more information can be found in the appendix. Pulsed laser deposition (PLD) was either carried out at finite oxygen partial pressure (oPLD) or in an inert gas atmosphere (iPLD). Reactive magnetron sputtering (RMS) from metallic

[9] Note that in the soft x-ray regime it is particularly difficult to sense the interface, since total electron yield measurements probe only the first few nanometres of the film (see Naftel and Sham [22]) and for the fluorescence yield a probing depth of approximately 100 nm can be achieved (see Henke *et al* [22]).

Zn/Co targets was used for growth under various oxygen partial pressures. For each type of fabrication method, we have chosen two distinct preparation conditions which lead either to PM or superparamagnetic (SPM) behaviour, as evidenced by SQUID measurements (see below). The PM-oPLD sample was discussed in [10]; although it has been Zn-diffused, XAS and SQUID results are identical to those for the as-grown specimen. The SPM-oPLD sample was prepared under similar conditions, including Zn-diffusion, but on Al_2O_3 $(01\bar{1}2)$ (r-plane sapphire) instead of $Al_2O_3(0001)$ (c-plane sapphire). The PM-iPLD sample was grown on c-plane sapphire, whereas the SPM-iPLD sample was deposited on ZnO(0001) under identical growth conditions. The PM-RMS sample was grown using an $Ar : O_2$ ratio of $10 : 1$ as the sputter gas, whereas the SPM-RMS sample was deposited with a reduced $Ar : O_2$ ratio of $10 : 0.5$, both on c-plane sapphire. In addition, a high-quality ZnO film was grown by molecular beam epitaxy (MBE) on c-plane sapphire and Co^+-ion implanted using implantation conditions which are known to lead to phase separation [30]. Note that it is also possible to fabricate PM-MBE samples by altered ion-implantation conditions. Since the absolute number of incorporated Co atoms had to be 15 times lower, however, we decided not to discuss the XLD because of increased noise. XMCD could not be recorded in this case, but SQUID magnetometry reveals PM.

Integral magnetic measurements were performed with a commercial SQUID magnetometer applying the magnetic field in the film plane. All relevant measurement artefacts (as described in greater detail in [31]) were carefully corrected; signals below 0.4 μemu were considered to be below the artefact level of the SQUID. The residual normalized magnetization at 300 K is always less than 1% of the 5 K magnetization for all PM samples; for all other magnetization data, the relative uncertainty is between 1 and 0.1% at magnetic fields larger than 1 T. $M(T)$ curves were measured while warming in a field of 10 mT, before the sample was either field cooled (FC) from 300 to 5 K in 4 T or zero-field cooled (ZFC) after demagnetizing the sample in an oscillatory field at 300 K. In all cases the diamagnetic contribution was derived from the $M(H)$ behaviour at high magnetic fields at 300 K and was subtracted from the data.

The XAS at the Co K-edge were taken at the ESRF beamline ID12 in total fluorescence yield [32]. For the XAS measurements at 300 K, a quarter wave plate [32] was used to flip the linear polarization of the synchrotron light from vertical (E-vector of the light $\parallel$ to the c-axis of the Co:ZnO) to horizontal ($E \perp c$); the angle of incidence was 10° with respect to the sample surface. The XLD was the direct difference of the XAS with $E \perp c$ and $E \parallel c$. The XANES was derived from the weighted average of the two spectra, i.e. $(2 \times \mathrm{XAS}(E \perp c) + \mathrm{XAS}(E \parallel c)/3$. The XMCD measurements were taken at 6 K as the direct difference of XANES spectra recorded with right and left circular polarized light under 15° grazing incidence in a magnetic field of ± 6 T.

XPS were recorded using a monochromatized Al K_α x-ray source ($h\nu = 1486.6$ eV). Depth profiles were taken after Ar-ion sputter ablation. Monochromatic x-ray diffractometry (XRD) was performed using a commercial high-resolution four-circle diffractometer (Bruker AXS D8 Discover). The device is equipped with a Göbel mirror to create a parallel x-ray beam and a Ge monochromator to provide monochromatic Cu $K_{\alpha 1}$ radiation ($\lambda = 1.540562$ Å). Non-monochromatic XRD measurements were taken with a Philips PANalytical X'Pert PRO using non-monochromatized Cu $K_{\alpha 1}$ and $K_{\alpha 2}$ radiation with a weighted average wavelength of 1.5418 Å together with an X'Celerator detector.

High-resolution transmission electron microscopy (HRTEM) was carried out using a Philips CM300UT field emission transmission electron microscope (FEG-TEM) equipped with an electron energy imaging filter (GIF, Gatan Inc.), and the TEM studies were conducted on specimens where the Co:ZnO thin films were prepared and viewed in cross section. The elemental maps of cobalt, zinc and oxygen were generated by energy-filtering TEM (EFTEM) using the three-window method [33] at the Co L-, Zn L-, and O K-ionization edges, respectively. For this investigation two single exposures of energy-filtered images, each taken with an exposure time of 80 s, were cross-correlated and averaged to obtain elemental maps with reduced noise.

3. Integral magnetic properties

Figure 1 shows a compilation of the integral magnetic data obtained by SQUID magnetometric measurements using an identical protocol for all seven samples. For ease of comparison, the displayed magnetization is normalized by the magnetization measured at 5 K and 4 T for each sample. The three PM samples exhibit identical $M(H)$ behaviour (figure 1(a)), devoid of any opening in the $M(H)$ curves at 5 K or any sizable magnetization at 300 K in excess of the detection limit of the SQUID instrument [31]. The $M(T)$ curves of the three PM samples (figure 1(b)) strongly overlap, revealing no separation between the FC and ZFC data. In contrast, the four SPM samples show clear hysteresis (figure 1(c)) at 5 K. The respective $M(H)$ curves recorded at 300 K (symbols in figure 1(d)) show a pronounced S-shape but are anhysteretic. They can be fitted well using a Langevin function (lines in figure 1(d)). Such a fit yields an average supermoment and an average particle diameter. We derive $5100\mu_B$ ($\sim$4 nm) for the SPM-MBE, $2500\mu_B$ ($\sim$3 nm) for the SPM-iPLD, $10\,000\mu_B$ ($\sim$5 nm) for the SPM-RMS, and $5000\mu_B$ ($\sim$4 nm) for the SPM-oPLD sample, where the particle diameters given in parentheses are calculated assuming the magnetic species is metallic hcp Co ($1.7\,\mu_B\,\mathrm{atom}^{-1}$). Although the S-shaped $M(H)$ curves are often attributed to a ferromagnetic state, they are actually indicative of SPM. Thus none of the samples is ferromagnetic at 300 K. The presence of SPM is further evidenced in figure 1(e), which summarizes the temperature-dependent magnetization data. Consistent with the $M(H)$ curves, the $M(T)$ dependencies show a clear separation between the FC and the ZFC curves and varying T values for the maxima in the ZFC-$M(T)$ behaviour. This behaviour is characteristic of an ensemble of SPM particles being blocked at low temperature [12]. We note that it is tempting to take the observation of hysteretic $M(H)$ curves at low T as evidence for bulk ferromagnetic order in the samples SPM-oPLD, SPM-iPLD, SPM-RMS and SPM-MBE. However, these data by no means constitute proof of intrinsic ferromagnetism. In contrast, ferromagnetism can be definitely ruled out for samples PM-oPLD, PM-iPLD and PM-RMS, as seen with other Co:ZnO samples of comparable high structural quality [9, 10] and confirmed by recent *ab initio* calculations [34]. The SQUID data provide the distinction between PM and SPM samples, which can be quantified by the ratio between the magnetization measured at 5 and 300 K at 4 T, respectively. The central yellow panel reveals that for all three PM samples, this ratio exceeds 100. Conversely, all four SPM samples fall below 20. However, the SQUID data alone cannot distinguish between ferromagnetic/SPM behaviour of a single-phase DMS that is intrinsic and that which results from extensive defects or secondary phase formation. For this, we turn to non-destructive XAS measurements.

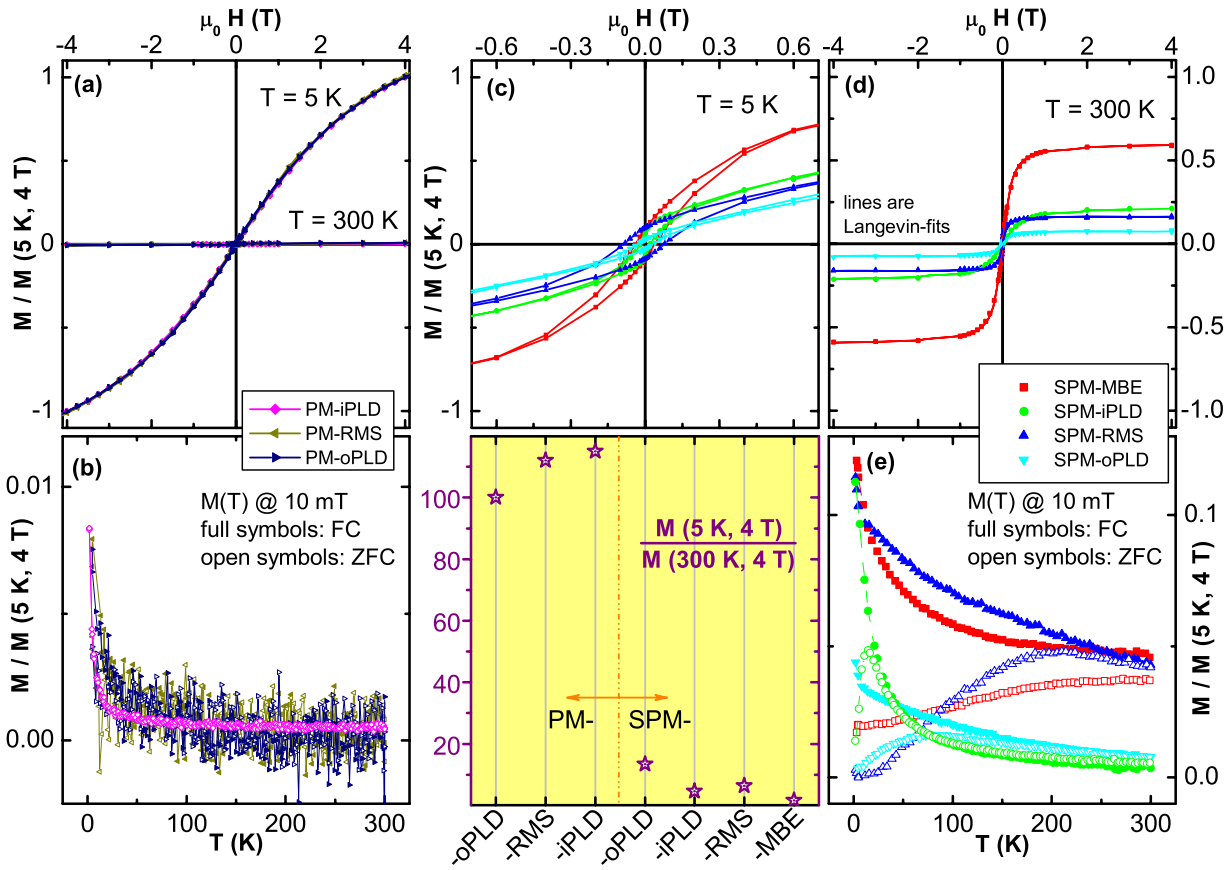

Figure 1. Integral magnetic properties of Co:ZnO measured by SQUID; all magnetization data have been normalized to the magnetization measured at 5 K and 4 T and the diamagnetic contribution of the substrate has been subtracted. (a) $M(H)$ curves recorded at 5 and 300 K for the three PM samples. (b) FC (in 4 T) versus ZFC curves measured while warming in 10 mT for the PM samples. (c) Magnification of the low-field $M(H)$ data at 5 K for the SPM samples. (d) $M(H)$ at 300 K together with a Langevin fit of the SPM samples revealing the anhysteretic $M(H)$ curves typical for SPM. (e) The FC/ZFC separation visible for the SPM samples exhibiting different blocking temperatures. The yellow panel illustrates the ratio of the normalized magnetization between 5 and 300 K data to distinguish between PM and SPM samples, the experimental uncertainty is smaller than the symbol size.

4. Element-specific x-ray investigation

To understand these materials at an atomistic level, measurements using synchrotron radiation in the hard x-ray regime were carried out. We first discuss the XANES and XLD data, which provide information on the electronic properties and the local structure of the Co dopant atoms. We will focus exclusively on the Co K-edge since the Zn K-edge spectra (not shown) do not exhibit any significant differences for all seven samples. Figure 2(a) compiles the seven normalized Co K-edge spectra together with a reference spectrum of a metallic foil of hcp Co.

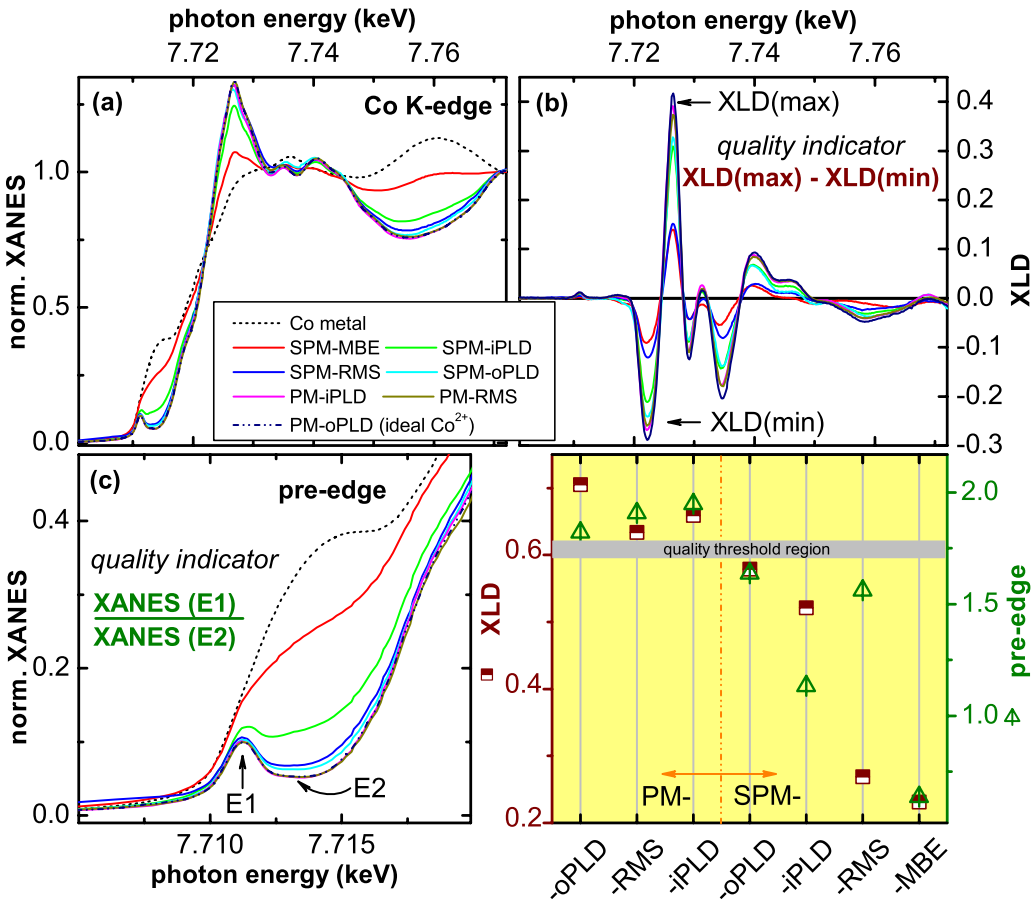

Figure 2. Local structure of Co:ZnO probed by XANES and XLD: (a) Normalized XANES spectra and (b) respective XLD signatures. (c) Enlarged pre-edge feature of the Co *K*-edge indicative of tetrahedrally coordinated Co^{2+}. The yellow panel displays the quality indicators based on the depth of the pre-edge feature and the size of the XLD for all seven samples; relative uncertainties are smaller than the symbol size.

While the three PM samples have identical spectra, there are clear differences in the spectra for the SPM samples. This is particularly true for the pre-edge feature enlarged in figure 2(c), which is associated with a $1s \rightarrow (3d, 4p)$ transition, as well as for the main peak, which is predominantly a $1s \rightarrow 4p$ transition. Differences are also visible in the onset of the EXAFS regime ($\gtrsim$7.73 keV). The spectra of all four SPM samples appear more 'metallic', i.e. they resemble the reference spectrum of metallic Co. To perform a more quantitative analysis of the data, the XLD signal was also recorded (figure 2(b)). The three PM samples yield a maximum XLD signal larger than 0.6 which, in comparison to data from [10], establishes that more than 95% of the Co dopant atoms are located on substitutional Zn lattice sites. We will in the following use the spectra of the PM-oPLD as reference spectra termed 'ideal' Co^{2+}, i.e. maximum substitution of Co dopant atoms on tetrahedrally coordinated Zn lattice sites. For the SPM samples, the XLD signal is reduced (figure 2(b)). This means that a smaller fraction of the Co atoms is on Zn sites, the remainder either being randomly positioned, or in some cubic or other non-wurtzite structure. Furthermore, the gap between the pre-edge feature and

the major onset of absorption starts to fill slightly for the SPM-oPLD and SPM-RMS samples, and is almost absent for the SPM-iPLD and SPM-MBE samples (figure 2(c)). From figure 2 we can derive two quality indicators (yellow panel):

(i) *The pre-edge feature (olive up triangles).* By dividing the maximum value of the normalized XANES at energy $E1$ by the XANES at the local minimum (energy $E2$), one derives a measure of the 'depth' of this feature. For the PM samples, this indicator exceeds 1.82, whereas for SPM samples it is lower than 1.65.

(ii) *The size of the XLD (wine half-filled squares).* All PM samples have an XLD signal exceeding 0.62. All four SPM samples have an XLD signal which falls below the threshold region from 0.62 to 0.59.

Note that the size of the XLD of SPM-oPLD reaches 85% of the maximum XLD signal of 0.71 measured for the PM-oPLD sample. This specimen has to be compared to the PM-RMS sample, which exhibits 90% of the ideal Co^{2+} XLD signal. These differences are significant, since the quality indicators rely on quasi-noise-free spectra so that the relative uncertainty for each sample is below 1%. Comparing different samples with each other, the XLD indicator becomes less sensitive in cases where only a small fraction of the sample is affected; in the present case, the Zn annealing affects only the topmost ∼10 nm of the SPM-oPLD sample [18], accounting for subtle changes in the value of the indicator. To yield quantitative information, XLD measurements have to be either combined with simulations as in [10, 23, 29], or a reference sample is required.

In figures 3(a)–(c) the residual XANES spectra of all SPM samples were determined by the following procedure. We used the ratio of the XLD signal for a given specimen to that of the PM-oPLD sample, which exhibited the largest XLD ('ideal' Co^{2+}). Then, the normalized XANES spectrum of the 'ideal' Co^{2+} was multiplied by the XLD ratio and subtracted from the experimental XANES spectrum. The residual XANES spectrum was then renormalized and contained the spectroscopic signatures of virtually all (more than ∼90%) Co atoms which were not in the 'ideal' Co^{2+} environment. Figure 3(a) displays the residual XANES for the SPM-RMS sample. The residual XANES is very similar to that of 'ideal' Co^{2+}, indicating the presence of rotated crystallographic grains, which in turn reduces the XLD but does not affect the XANES. Figure 3(b) shows the residual XANES of the SPM-oPLD sample. Its fine structure exhibits four distinct peaks which resemble neither metallic Co nor 'ideal' Co^{2+}. This result suggests a modified electronic state of the Co and thus may provide evidence for phase separation. Figure 3(c) demonstrates that the residual XANES signal of the SPM-iPLD and SPM-MBE samples are almost identical to metallic hcp Co. Taking into account the size of the XLD, 26% of the Co in SPM-iPLD and 67% in SPM-MBE is present as elemental (metallic-like) Co(0). This can easily account for the observed integral magnetic properties of the two samples. Finally, figure 3(d) shows an enlarged view of the $1s \rightarrow (3d, 4p)$ pre-edge feature of the residual XANES spectra of all four SPM samples. These data clearly demonstrate the increasing elemental character for Co atoms not substitutionally located on Zn sites in going from SPM-RMS to SPM-oPLD to SPM-iPLD to SPM-MBE.

We next turn to the XMCD data to gain element-specific information regarding the magnetic properties. Figure 4(a) shows spectra recorded at the Co K-edge at 6.5 K of all three PM samples. These spectra are virtually identical. Element-specific XMCD(H) curves recorded at the photon energy of the pre-edge feature corroborate the PM behaviour of these samples (not shown, see [10] for the PM-oPLD). Note that the size of the XMCD signal for the

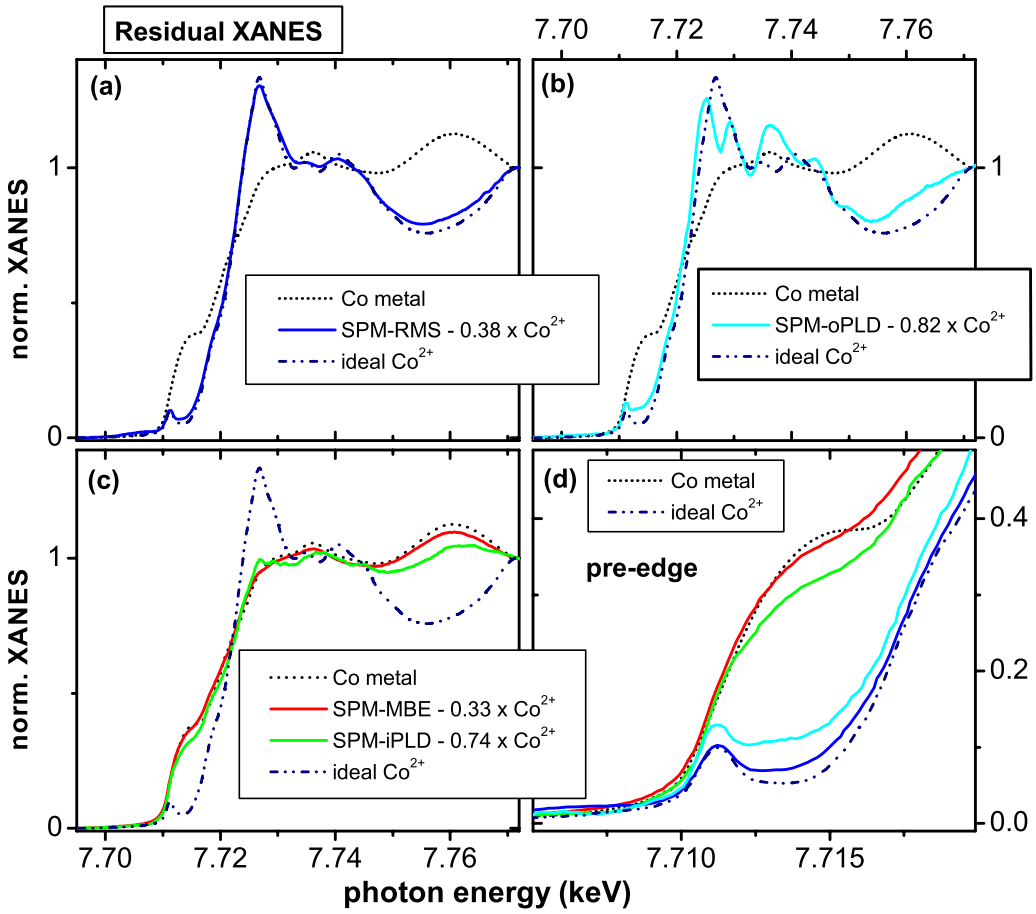

Figure 3. Residual XANES signatures of SPM-Co:ZnO: the residual (see text) XANES spectra of (a) the SPM-RMS sample, (b) the SPM-oPLD sample, (c) the SPM-iPLD and SPM-MBE samples, revealing the spectroscopic signatures of the phase-separated material. (d) Enlarged pre-edge region of the residual XANES revealing increasing elemental Co(0) character.

PM-iPLD sample has been corrected for the lower Co content (5%) since isolated Co dopant atoms contribute most strongly to the XMCD signal, whereas Co–O–Co pairs (which occur more frequently in the 10% Co-doped than the 5% Co doping samples) couple antiparallel and do not contribute to the XMCD in these experimental conditions (6.5 K and 6 T) [10, 11]. In figure 4(b), an XMCD spectrum for metallic hcp Co is shown, together with the XMCD of the SPM-MBE sample recorded at 250 K. At this temperature the PM contribution to the signal of the SPM-MBE sample is negligible due to the $1/T$ temperature dependence, thus corroborating a large fraction of magnetically active elemental Co in this sample. The two 'metallic' XMCD spectra in figure 4(b) demonstrate that at the photon energy where the XMCD has its maximum negative signal, the XMCD of 'ideal' Co^{2+} (shown for comparison) is virtually zero. A growing XMCD signal at this energy therefore indicates an increasing fraction of magnetically active elemental Co(0) in a given specimen. Figures 4(c)–(e) show the XMCD spectra for the SPM-oPLD, the SPM-RMS and the SPM-iPLD samples, respectively. A clear reduction of the XMCD at the pre-edge feature is visible, especially for the SPM-RMS sample.

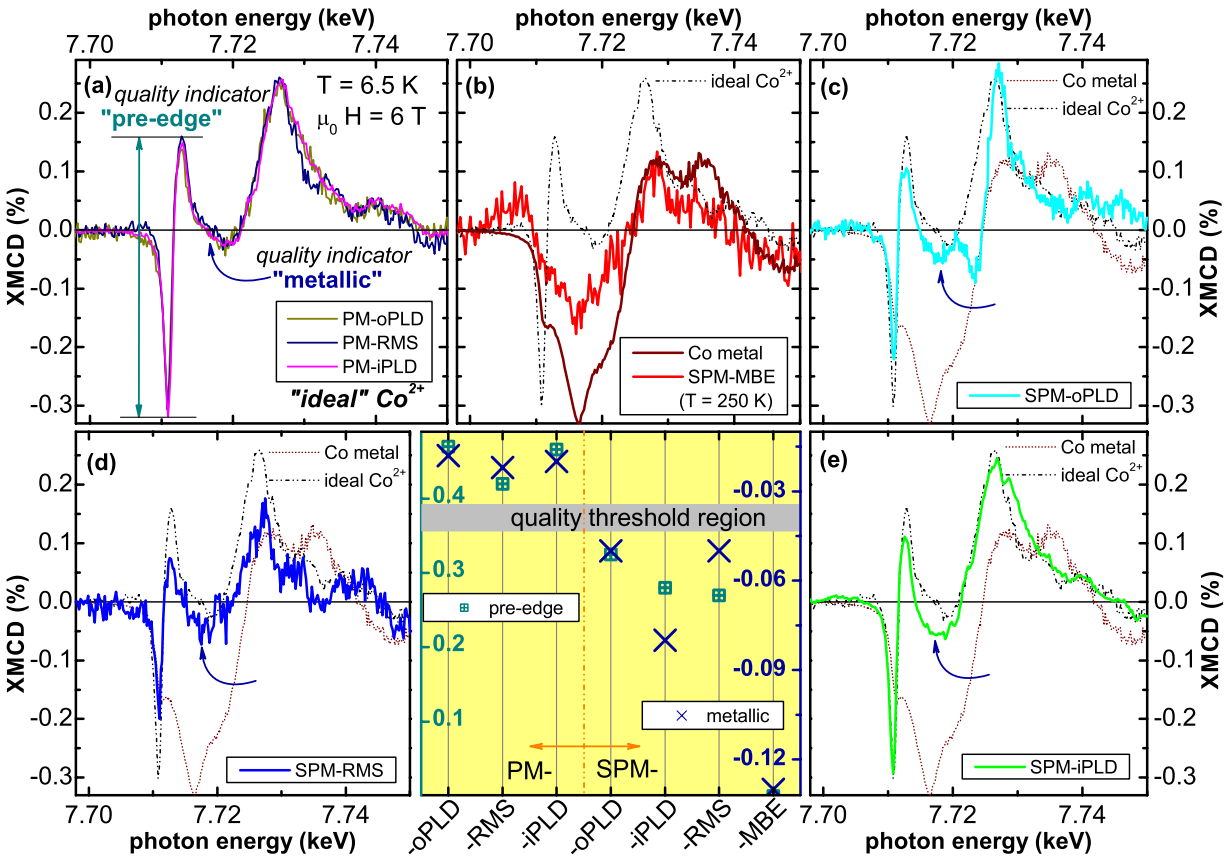

Figure 4. Element-specific magnetism for Co in Co:ZnO. (a) XMCD spectra of the three PM samples measured at 6.5 K. (b) XMCD of a metallic hcp Co reference sample at 6.5 K, together with the XMCD of the SPM-MBE sample measured at 250 K. XMCD spectra at 6.5 K of (c) the SPM-oPLD, (d) the SPM-RMS and (e) the SPM-iPLD sample. The yellow panel shows the quality indicators (pre-edge and 'metallic' as indicated in (a)) based on XMCD for all seven specimens. The absolute uncertainty of these indicators can be estimated from the noise of the respective XMCD spectra before the edge, i.e. between 0.01 and 0.03%.

In addition, the SPM-oPLD and SPM-iPLD show a significant increase in the 'metallic' XMCD signal. Note that the XMCD of the SPM-iPLD sample has been corrected for the lower Co content as well. Figure 4 suggests the introduction of two additional quality indicators based on the XMCD spectra (yellow panel):

(i) *The peak-to-peak amplitude of the XMCD signal at the pre-edge feature (crossed squares).* The three PM samples consistently exhibit a dichroic signal of 0.42–0.47% (figure 3(a)).

(ii) *The magnitude of the 'metallic' XMCD (crosses).* The size of the XMCD at the photon energy where Co metal has its maximum negative XMCD signal. Whereas the three PM samples have an almost zero (within the noise) XMCD signal, at most above −0.03%, all SPM samples have an XMCD clearly below −0.05%.

The size of the above XMCD quality indicators are consistent with the hard XMCD spectrum for ferromagnetic-like 25% Co in ZnO shown in [27], where a metallic Co phase was evidenced in combination with soft XMCD, as well as with the XMCD findings for PM 7% Co-doped ZnO nanorods in [28]. Note that both XMCD quality indicators depend on the Co concentration, since the fraction of antiferromagnetically coupled Co atoms does not contribute to the XMCD signal. In contrast, the XLD indicator depends only on the reduced local symmetry of the lattice sites and is independent of magnetic interactions.

By combining the XLD spectra in figure 2, the residual XANES spectra in figure 3 and the XMCD spectra in figure 4, we derive the following generalizations. (i) All three deposition techniques (RMS, iPLD and oPLD) can result in Co:ZnO samples where the Co is predominantly located substitutionally on tetrahedral Zn lattice sites. Such samples have characteristic spectral features in XANES and XMCD as well as a large XLD signal above 0.62. These samples are all PM as seen in figure 1. (ii) The relative reduction of the XLD with respect to the 'ideal' Co^{2+} allows us to extract a residual XANES for the four SPM samples, providing further clues on the nature of the fraction of Co atoms not ideally incorporated in ZnO. (iii) The oxidizing preparation conditions for the SPM-RMS sample obviously lead predominantly to a Co–O compound secondary phase as evidenced by the residual XANES; the reduced XMCD signal points towards an antiferromagnetic compound. (iv) The Zn-annealing treatment of the SPM-oPLD sample leads to a drastically altered fine structure and more elemental Co(0) character. (v) The SPM-iPLD and SPM-MBE samples show clear indications of elemental Co(0) in the residual XANES and XMCD spectra.

5. Evidence for phase separation

Figure 5 summarizes complementary x-ray-based experimental evidence for phase separation in the SPM samples. Figure 5(a) shows an XPS spectrum at the Co $2p_{3/2}$ and Co $2p_{1/2}$ emission lines in the vicinity of the surface of the SPM-oPLD film, i.e. after removal of the topmost 4.5 nm by sputtering. Clear additional peaks at lower binding energies are visible, which are characteristic of elemental Co(0). The XPS spectrum is fitted to a superposition of Co^{2+} and Co(0), clearly corroborating the previous findings for increased elemental character of the Co close to the surface. The XPS depth profile (not shown, see [18]) demonstrates that the elemental Co(0) is located only near the surface of the film. The Co(0) enrichment at the surface originates from the Zn-diffusion of SPM-oPLD, since no signs of elemental Co(0) were found in the as-grown sample (figure 5(a), dashed line). Note that a detailed EXAFS analysis also revealed the formation of a CoZn intermetallic compound in a similar sample (see [18]).

Figures 5(b)–(d) show complementary evidence for additional crystallographic phases in the SPM-RMS and SPM-iPLD samples by means of XRD. By drastically increasing the integration time of an $\omega - 2\theta$ scan, a broad reflection around $2\theta = 44^\circ$ becomes visible for the SPM-iPLD sample, which is absent for the PM-iPLD sample (figure 5(b)). In this region, one expects reflections for fcc and hcp metallic Co as well as Co_3O_4 and $ZnCo_2O_4$ spinel. While the large full-width at half-maximum (FWHM) for this reflection precludes a positive identification, the XANES in figure 3(c) suggests Co(0) rather than an oxide compound. Figure 5(c) shows the XRD of the PM-RMS sample using a high-flux powder diffractometer around 36.5°, where both CoO and reflections for rotated grains of ZnO are expected; the region around 44° is shown in figure 5(d). While a clear reflection can be seen in the former region, an additional reflection in the latter region is faint. This is in agreement with the XANES/XLD data, which indicate

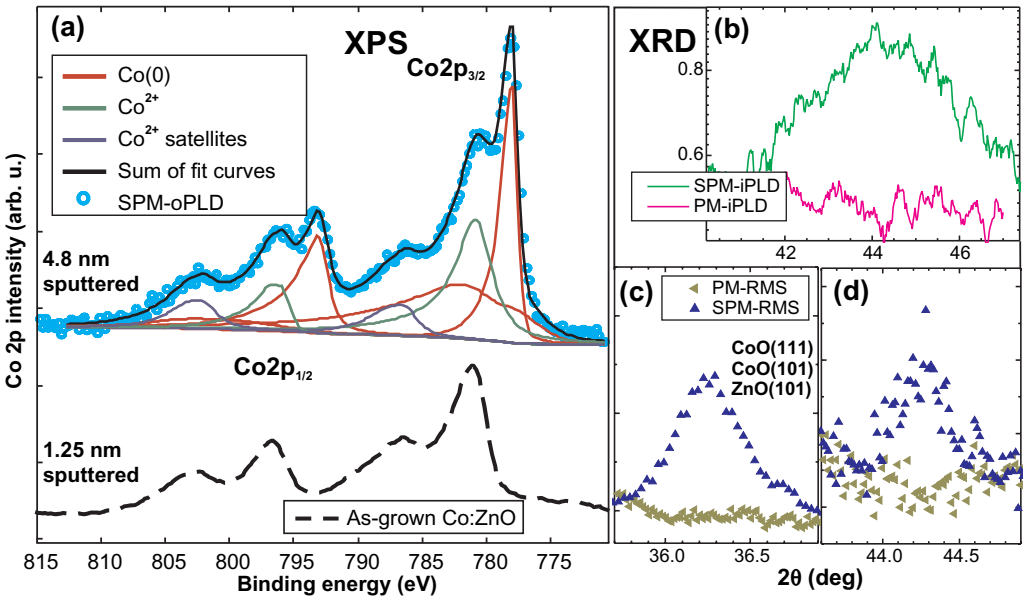

Figure 5. Phase separation in the SPM samples. (a) Fit of an XPS spectrum of SPM-oPLD after sputter removal of the topmost 4.5 nm of the film to a superposition of Co^{2+} and Co(0), revealing a fraction of metallic Co. For comparison an XPS spectrum for the as-grown sample after removal of the topmost 1.25 nm is shown. (b) $\omega - 2\theta$ XRD scans revealing an additional reflection for the SPM-iPLD sample, which is absent from the PM-iPLD sample. (c) and (d) show additional reflections for the SPM-RMS samples which are absent from the PM-RMS specimen.

that in the SPM-RMS sample a Co–O compound and a small fraction of elemental Co are the dominant secondary phases, rather than cubic CoO or Co_3O_4. For comparison, the PM-RMS sample is shown as well, and there is no evidence for secondary phases in this specimen.

Figures 6(a)–(d) show direct experimental evidence for phase separation in the SPM-iPLD sample by means of TEM and EFTEM [33]. In figure 6(a), a TEM image of the sample in cross section is displayed with one nano-crystal visible. The crystallite diameter is approximately 4 nm, consistent with the estimation of the Langevin fit in figure 1(d), making such nanoclusters difficult to detect by XRD (see figure 5(b)). The elemental maps of the same region obtained by EFTEM demonstrate that this phase-separated nanocrystal is rich in Co (figure 6(b)), but deficient in Zn (c) and oxygen (d). These data thus constitute direct evidence that the residual elemental Co(0) found by XANES/XMCD is present in the form of phase-separated metallic Co clusters, and can readily explain the integral magnetic properties as measured by SQUID. Note that XMCD spectra at the Co L_3-edge were also recorded for the SPM-iPLD sample and indicate that the largest fraction of elemental Co is located far away from the surface and well inside the bulk of the thin film (see figure 3(e)–(f) in [12]). Thus, the imaging of a single nanocluster by TEM is not necessarily representative of the distribution of inclusions in the film.

From figures 5 and 6, it is obvious that phase separation occurs in all SPM samples, including MBE, see [30]. The additional phase is either Co–O (RMS), metallic CoZn (oPLD) or

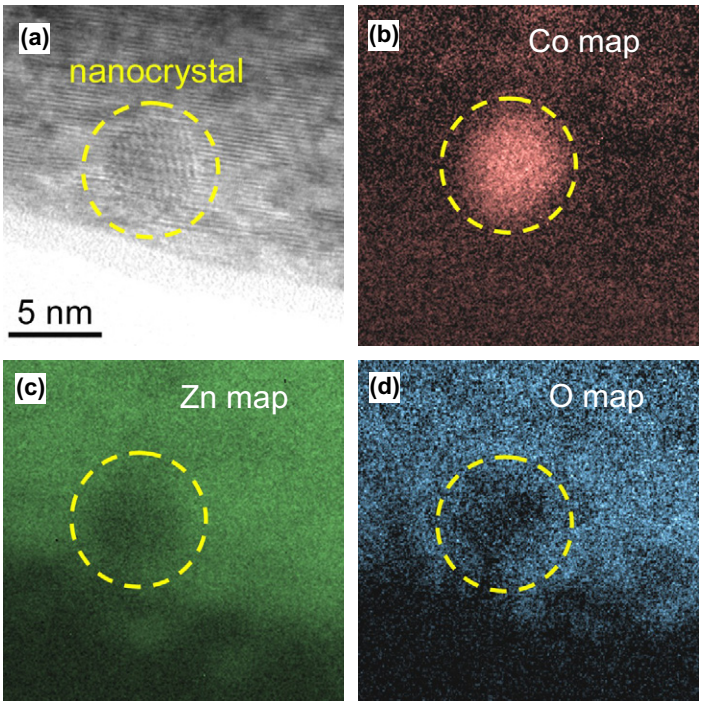

Figure 6. Metallic Co nanoclusters in the SPM-iPLD sample. (a) HRTEM image revealing a nanocrystal with a diameter of about 4 nm. This region is rich in Co (b), but deficient in Zn (c) and oxygen (d), as demonstrated by EFTEM.

Co (iPLD, MBE). These phases can be located either close to the surface (figure 5(a)), e.g. after Zn annealing treatment, or in the bulk. The complementary materials characterization methods used to detect phase separation in the SPM samples are laborious, potentially insensitive to low concentrations of secondary phases, and often destructive. In contrast, hard x-ray-based XAS techniques offer the advantage that the entire film thickness can be probed up to 500 nm and beyond non-destructively. We want to stress that for all three preparation techniques it was possible to fabricate both intrinsic PM and phase-separated SPM samples. The differences in preparation between PM and SPM were minor: (i) a reduction of the oxygen content in the sputter gas (RMS) intended to alter the carrier concentration, see [35], (ii) a change of substrate from sapphire to ZnO (iPLD) to improve the crystallinity or (iii) a change in the orientation of the sapphire substrate from *c*- to *r*-plane sapphire (oPLD). It should be noted that the transition from PM to SPM in the oPLD samples is not caused by an altered carrier concentration due to the Zn diffusion, but stems from an increased in-diffusion of Zn and subsequent reduction of substitutional Co^{2+} for films grown on *r*-plane sapphire. Similarly, the PM to SPM transition between the two iPLD samples is solely caused by the choice of the substrate. Evidently, deposition of relaxed films on sapphire leads to PM and substitutional Co^{2+} on Zn sites, whereas lattice-matched growth on ZnO results in SPM and a considerable fraction of elemental Co(0). We attribute this to the reduced stability of ZnO compared to sapphire at the given growth conditions, resulting in more extensive ZnO decomposition and the attendant generation of elemental Zn, which in turn reduces substitutional Co^{2+}.

6. Summary

Advanced synchrotron-based spectroscopy at the Co *K*-edge can provide a direct and sensitive probe of specimen quality and thus substantiate or refute claims of intrinsic ferromagnetism in a meaningful manner. We have introduced four different quantitative quality indicators based on XANES and XLD (figure 2), and on XMCD (figure 4), which allow us to directly distinguish between tetrahedrally coordinated Co^{2+} on Zn lattice sites and phase-separated Co–O, CoZn intermetallics and elemental Co(0). Specimens that meet the quality thresholds are devoid of secondary phases and are consistently PM. When the four quality indicators fall below the threshold, phase separation can be proven. We have demonstrated that even slight changes in the preparation conditions of Co:ZnO can promote the onset of phase separation, revealing an extrinsic origin of the observed SPM in all cases. Utilizing XAS to reconcile magnetic properties with phase purity is a powerful approach, which can be generalized in a straightforward manner to other dilute/doped oxides and nitrides.

Acknowledgments

We are very grateful to T Wassner and M Eickhoff from the Walter-Schottky Institute, Garching, for providing us with the MBE-grown ZnO film for the Co-ion implantation. We thank Andreas Erb for the careful preparation of the polycrystalline target materials for the PLD process at the WMI. The work at the UDE was supported by the European Union under the Marie-Curie Excellence Grant No. MEXT-CT-2004-014195 of the 6th Framework Programme; hosting of the project by Professor Farle is gratefully acknowledged. The work at the WMI was supported by the Deutsche Forschungsgemeinschaft via SPP 1157 (project GR 1132/13), SPP 1285 (project GR 1132/14) and the Nanosystems Initiative Munich (NIM). A portion of the research was performed using EMSL, a national scientific user facility sponsored by the Department of Energy's Office of Biological and Environmental Research located at Pacific Northwest National Laboratory. The work in Bonn was supported by the Deutsche Forschungsgemeinschaft via SPP 1157 (project MA 1020/11). Use of the Advanced Photon Source was also supported by the U.S. Department of Energy, Office of Science, Office of Basic Energy Sciences, under Contract DE-AC02-06CH11357.

Appendix. Details of sample preparation

oPLD samples. $Co_{0.1}Zn_{0.9}O(0001)$ epitaxial films were grown at PNNL by off-axis PLD from CoO/ZnO ceramic targets. The PM-oPLD sample was grown on epiready $Al_2O_3(0001)$ substrates (*c*-plane sapphire) at a substrate temperature of 550 °C and an O_2 pressure of 10 mTorr. The KrF-laser repetition rate was 1 Hz with a fluence of 2.4 J cm^{-2} incident on the target. Non-monochromatic XRD indicates high structural quality with a FWHM of 0.38° in ω-rocking curves of the (0002) reflection of ZnO, which itself has a FWHM of less than 0.15° in the $\omega - 2\theta$ scan. The SPM-oPLD sample was grown on $Al_2O_3(01\bar{1}2)$ (*r*-plane sapphire) at a substrate temperature of 475 °C and an O_2 pressure of 1 mTorr. The laser repetition rate was 5 Hz with a fluence of 2.4 J cm^{-2} incident on the target. XRD indicates high structural perfection with a FWHM of less than 0.15° in the $\omega - 2\theta$ scan of the (110) reflection of ZnO. Both oPLD samples were annealed at 600 °C in Zn atmosphere for 5 h [18].

iPLD samples. Nominally $Co_{0.05}Zn_{0.95}O(0001)$ epitaxial thin films were grown at the WMI by on-axis PLD from a stoichiometric ceramic CoO/ZnO target. The PM-iPLD and the SPM-iPLD samples were grown on epiready *c*-plane sapphire and ZnO(0001) substrates, respectively, at a substrate temperature of 400 °C in an inert Ar atmosphere of 4×10^{-3} mbar. The KrF-laser repetition rate was 2 Hz yielding 2 J cm^{-2} incident on the target. The growth was monitored *in situ* by reflection high energy electron diffraction (RHEED). Monochromatic XRD indicates high structural quality with an FWHM of the rocking curves of 0.016° (SPM-iPLD) and slightly reduced quality with an FWHM of 0.2° (PM-iPLD), respectively.

RMS samples. Nominally $Co_{0.1}Zn_{0.9}O(0001)$ epitaxial films were grown at the UDE on epiready *c*-plane sapphire substrates using reactive dc-magnetron sputtering (RMS) from metal targets in an ultrahigh vacuum deposition system with a base pressure of 5×10^{-10} mbar and a substrate temperature of 350 °C. The pressure during deposition was 4×10^{-3} mbar and the $Ar : O_2$ ratio was varied from 10:1 (PM-RMS) down to 10:0.5. (SPM-RMS). XRD indicates good structural quality for the PM-RMS sample with a FWHM of 0.75° in ω-rocking curves of the (0002) reflection of ZnO, which itself has a FWHM of less than 0.15° in the $\omega - 2\theta$ scan.

SPM-MBE sample. Undoped ZnO was grown on an 20 nm Mg:ZnO buffer layer on *c*-plane sapphire substrates by MBE under RHEED control at the Walter-Schottky Institute. It has excellent structural quality as indicated by the FWHM of 0.007° in ω-rocking curves of the (0002) reflection of ZnO, which itself has a FWHM of 0.03° in the $\omega - 2\theta$ scan. It was Co^+-ion implanted at 350 ° C at the FZ Dresden-Rossendorf with an ion energy of 180 keV and a fluence of 5×10^{16} cm^{-2}. This implantation process is known to yield phase-separated metallic Co clusters [30].

References

[1] Sato K, Fukushima T and Katayama-Yoshida H 2007 *Jpn. J. Appl. Phys.* **46** L682 and refs. therein
[2] Sato K and Katayama-Yoshida H 2000 *Jpn. J. Appl. Phys.* **39** L555
[3] Ueda K, Tabata H and Kawai T 2001 *Appl. Phys. Lett.* **79** 988
[4] Coey J M D, Venkatesan M and Fitzgerald C B 2005 *Nat. Mater.* **4** 173
[5] Kittilstved K R, Liu W K and Gamelin D R 2006 *Nat. Mater.* **5** 291
[6] Behan A J, Mokhtari A, Blythe H J, Score D, Xu X-H, Neal J R, Fox A M and Gehring G A 2008 *Phys. Rev. Lett.* **100** 047206
[7] Akdogan N, Nefedov A, Westerholt K, Zabel H, Becker H-W, Somsen C, Khaibullin R and Tagirov L 2008 *J. Phys.* D **41** 165001
[8] Liu Y and MacManus-Driscoli J L 2009 *Appl. Phys. Lett.* **94** 022503
[9] Kaspar T C, Droubay T, Heald S M, Nachimuthu P, Wang C M, Shutthanandan V, Johnson C A, Gamelin D R and Chambers S A 2008 *New J. Phys.* **10** 055010
[10] Ney A, Ollefs K, Ye S, Kammermeier T, Ney V, Kaspar T C, Chambers S A, Wilhelm F and Rogalev A 2008 *Phys. Rev. Lett.* **100** 157201
[11] Sati P, Deparis C, Morhain C, Schäfer S and Stepanov A A 2007 *Phys. Rev. Lett.* **98** 137204
[12] Opel M, Nielsen K-W, Bauer S, Goennenwein S T B, Cezar J C, Schmeisser D, Simon J, Mader W and Gross R 2008 *Eur. Phys. J.* B **63** 437
[13] Barla A *et al* 2007 *Phys. Rev.* B **76** 125201
[14] Tietze T, Gacic M, Schütz G, Jakob G, Brück S and Goering E 2008 *New J. Phys.* **10** 055009
[15] Wi S C *et al* 2004 *Appl. Phys. Lett.* **84** 4233
[16] Wei H, Yao T, Pan Z, Mai C, Sun Z, Wu Z, Hu F, Jiang Y and Yan W 2009 *J. Appl. Phys.* **105** 043903

[17] Venkatesan M, Stamenov P, Dorneles L S, Gunning R D, Bernoux B and Coey J M D 2007 *Appl. Phys. Lett.* **90** 242508
[18] Kaspar T C, Droubay T, Heald S M, Engelhard M H, Nachimuthu P and Chambers S A 2008 *Phys. Rev.* B **77** 201303
[19] Ahlers S, Bougeard D, Sircar N, Abstreiter G, Trampert A, Opel M and Gross R 2006 *Phys. Rev.* B **74** 214411
[20] Jaeger C, Bihler C, Vallaitis T, Goennenwein S T B, Opel M, Gross R and Brandt M S 2006 *Phys. Rev.* B **74** 045330
[21] Dürr H A *et al* 2009 *IEEE Trans. Magn.* **45** 15
[22] Naftel S J and Sham T K 1999 *J. Synchrotron Radiat.* **6** 526
Henke B L, Lee P, Tanaka T J, Shimabukuro R L and Fujikawa B K 1982 *At. Data Nucl. Data Tables* **27** 1
[23] Sarigiannidou E, Wilhelm F, Monroy E, Galera R M, Bellet-Amalric E, Rogalev A, Goulon J, Cibert J and Mariette H 2006 *Phys. Rev.* B **74** 041306
[24] Martinez-Criadoa G, Segura A, Sans J A, Homs A, Pellicer-Porres J and Susini J 2006 *Appl. Phys. Lett.* **89** 061906
[25] Heald S M *et al* 2009 *Phys. Rev.* B **79** 075202
[26] Kobayashi M *et al* 2005 *Phys . Rev.* B **72** 201201
[27] Rode K *et al* 2008 *Appl. Phys. Lett.* **92** 012509
[28] Büsgen T, Hilgendorff M, Irsen S, Wilhelm F, Rogalev A, Goll D and Giersing M 2008 *J. Phys. Chem.* C **112** 2412
[29] Ney A, Kammermeier T, Manuel E, Ney V, Dhar S, Ploog K H, Wilhelm F and Rogalev A 2007 *Appl. Phys. Lett.* **90** 252515
[30] Zhou S, Potzger K, von Borany J, Grötzschel R, Skorupa W, Helm M and Fassbender J 2008 *Phys. Rev.* B **77** 035209
[31] Ney A, Kammermeier T, Ney V, Ollefs K and Ye S 2008 *J. Magn. Magn. Mater.* **320** 3341
[32] Rogalev A, Goulon J, Goulon-Ginet C and Malgrange C 2001 *Lect. Notes Phys.* **565** 61
[33] Hofer F, Warbichler P and Grogger W 1995 *Ultramicroscopy* **59** 15
[34] Nayak S K, Ogura M, Hucht A, Akai H and Entel P 2009 *J. Phys.: Condens. Matter* **21** 064238
[35] Ye S, Ney V, Kammermeier T, Ollefs K, Zhou S, Schmidt H, Wilhelm F, Rogalev A and Ney A 2009 *Phys. Rev.* B **80** 245321